Energy based Footstep Planning of Biped on Uneven Deformable Terrain using Nonlinear Inverted Pendulum

Sunil Gora *
Department of
Mechanical Engineering,
Indian Institute of Technology, Kanpur,
Uttar Pradesh, India, 208016
Email: sunilg@iitk.ac.in

Shakti S Gupta
Department of Mechanical Engineering,
Indian Institute of Technology, Kanpur,
Uttar Pradesh, India, 208016
Email: ssgupta@iitk.ac.in

Ashish Dutta
Department of Mechanical Engineering
Indian Institute of Technology, Kanpur
Uttar Pradesh, India, 208016
Email: adutta@iitk.ac.in

ABSTRACT

In this work, the motion of a Nonlinear Inverted Pendulum (NIP) on deformable terrain due to foot contact forces is used for energy analysis and footstep placement. In order to include the linear and rotational motions of the NIP, the mass moment of inertia of the body is also considered in the Center of Mass (CoM) model. The terrain deformation is modeled using a spring-damper contact model, and based on the rigid body dynamics of the NIP, its motion is generated. The energy analysis of the system provides the regions of possible foot placement. Based on the loss of potential energy due to ground deformation, the limits of terrain stiffness are also obtained for walking on uneven deformable terrain.

*Address all correspondence to this author.

1 INTRODUCTION

The locomotion of bipedal robots is classified into active and passive walking. In active walking, the motion is actively controlled by actuators with constraints such as Zero Moment Point (ZMP) [1] for stable biped gait. ZMP is used in simplified or reduced dynamics models such as Linear Inverted Pendulum Model (LIPM) [2], in which the Center of Mass (CoM) motion is constrained in a plane to generate stable gait on 3D flat terrain [3]. There have been significant contributions on biped walking over stairs [4], inclined slope [5], and uneven terrain [6], and the simplicity of LIPM has driven many control strategies for robot walking on 3D terrain [7]. LIPM is also extended to account the leg movements by considering the body inertia of the robot for a momentum based controller design [8] and push recovery [9]. On the other hand, passive walkers generate motion based on gravity, inertia and system's energy which includes kinetic and potential energy exchange [10]. The Nonlinear Inverted Pendulum (NIP) model is used to simplify the biped dynamics by considering fixed distance between center of mass and center of pressure [11]. The leg transition generates impact forces, hence footstep planning is crucial for energy optimal walking in passive walkers [12]. The foot placement position at which the kinetic energy vanishes at an unstable equilibrium of the inverted pendulum is called capture point [13]. The capture point of LIPM is extended for passive walking of NIP on hard uneven terrain [14].

The unstructured outdoor terrains such as grass, sand and soft clay may not provide sufficient forces to support the robot motion generated by LIPM or NIP model [15]. Such cases are addressed by modifying the controller based on small ground deformation [16, 17]. The floating-base dynamics of biped is also used to consider the ground deformation in contact dynamics [18], however, a predefined reference trajectory for walking gait on hard terrain is considered. Passive dynamic walking generates a human-like gait, and for energy-efficient walking on different types of terrains, the passive walker is more robust to disturbances due to the terrain than active walking models such as LIPM [19]. For walking on deformable terrain, the existing passive walkers focus on linear motion of the center of mass with fixed contact point [20]. The CoM model can be extended to a rigid body with mass moment of inertia for rotational motion due to foot contact forces acting at the moving contact point.

In this work, we propose a footstep planning based on the terrain properties. The contact forces provided by the foot-terrain interaction can be used in rigid body dynamics to consider the ground deformation as well [21]. For this work, NIP model is used with contact forces to analyze the energy regions for foot placement. The salient contributions of this work are as follows: 1.) Biped gait generation using linear and rotational motions of NIP considering foot contact forces on deformable terrain, 2.) Identification of the energy regions for footstep planning using the terrain properties and deformation of ground, and 3.) Terrain stiffness limits for walking forward on an uneven terrain.

The rest of the paper is organized as follows: The simplified dynamics of the robot, contact model and expressions for system's energies are presented in Section 2. In Section 3, the stance leg transition with kinematics and energy is shown. The energy regions such as capture curve and equal local energy curve are generated in Section 4. The results of the effect of ground deformation and variation of the energy region with the known terrain properties are presented in Section 5. Finally, the conclusions are given in Section 6.

2 SYSTEM MODELING AND DYNAMICS

As shown in Fig. 1, the biped is modeled as NIP of mass m and mass moment of inertia about y-axis passing through CoM I_{yy}. The fixed distance of CoM from the contact point is L. The pendulum has linear and rotational motions due to the planer contact forces F_x and F_z, gravitational acceleration g and system's energy E. The coordinates of the CoM in terms of position of the foot contact point (x, z) and orientation of the pendulum θ, are given by

$$\begin{bmatrix} x_c \\ z_c \end{bmatrix} = \begin{bmatrix} x \\ z \end{bmatrix} + L \begin{bmatrix} \cos\theta \\ \sin\theta \end{bmatrix}. \tag{1}$$

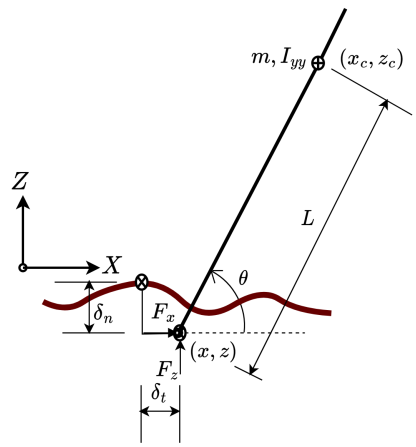

Fig. 1. NIP with ground deformation δ_n and δ_t in normal and tangential direction, respectively

The linear velocity of CoM by differentiation of Eq. (1) is obtained as

$$\begin{bmatrix} \dot{x}_c \\ \dot{z}_c \end{bmatrix} = \begin{bmatrix} \dot{x} \\ \dot{z} \end{bmatrix} + L\dot{\theta} \begin{bmatrix} -\sin\theta \\ \cos\theta \end{bmatrix}. \tag{2}$$

Similarly, the CoM accelerations can be written as

$$\begin{bmatrix} \ddot{x}_c \\ \ddot{z}_c \end{bmatrix} = \begin{bmatrix} \ddot{x} \\ \ddot{z} \end{bmatrix} + L\ddot{\theta} \begin{bmatrix} -\sin\theta \\ \cos\theta \end{bmatrix} - L\dot{\theta}^2 \begin{bmatrix} \cos\theta \\ \sin\theta \end{bmatrix}. \tag{3}$$

Given the foot contact forces F_x and F_z, the equations of motion are written as

$$m\ddot{x}_c = F_x, \tag{4}$$

$$m\ddot{z}_c = F_z - mg, \tag{5}$$

$$I_{yy}\ddot{\theta} = F_x L \sin\theta - F_z L \cos\theta. \tag{6}$$

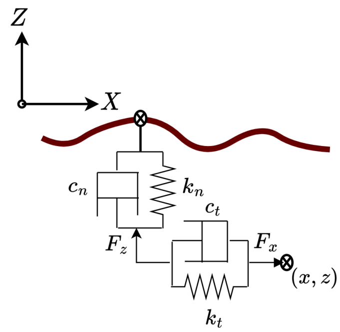

Fig. 2. Spring-damper contact model with terrain stiffness denoted by k_n in normal direction, k_t in tangential direction, and damping is denoted by c_n in normal direction and c_t in tangential direction

Substituting the expression of accelerations of CoM, we obtain the equations of motion as

$$\begin{bmatrix} m & 0 & -mL\sin\theta \\ 0 & m & mL\cos\theta \\ -mL\sin\theta & mL\cos\theta & I_{yy}+mL^2 \end{bmatrix} \begin{bmatrix} \ddot{x} \\ \ddot{z} \\ \ddot{\theta} \end{bmatrix} = \begin{bmatrix} F_x + mL\dot{\theta}^2\cos\theta \\ F_z - mg + mL\dot{\theta}^2\sin\theta \\ -mgL\cos\theta \end{bmatrix}. \tag{7}$$

Considering the contact forces, the motion of the pendulum is obtained.

2.1 Contact Modeling

The foot-terrain interaction is modeled using a spring and a damper as shown in Fig. 2. Considering the displacement and relative velocity of the contact point on pendulum with respect to ground in normal direction δ_n and $\dot{\delta}_n$, respectively, the normal contact force F_z is given by

$$F_z = \begin{cases} -k_n\delta_n - c_n\dot{\delta}_n, & \delta_n < 0 \;\&\; \dot{\delta}_n < 0, \\ -k_n\delta_n, & \delta_n < 0 \;\&\; \dot{\delta}_n \geq 0, \\ 0, & \delta_n \geq 0. \end{cases} \tag{8}$$

The displacement and relative velocity of the contact point in tangential direction are δ_t and $\dot{\delta}_t$, respectively. The tangential force F_x is given by

$$F_x = \begin{cases} -k_t\delta_t - c_t\dot{\delta}_t, & |F_x| < \mu F_z, \\ \pm\mu F_z, & |F_x| \geq \mu F_z. \end{cases} \tag{9}$$

Here, μ is the coefficient of friction, which is assumed to be sufficiently high for No-slip condition. The work done due to the contact forces in the contact time interval T is

$$W_c = \int_0^T (F_x\dot{\delta}_t + F_z\dot{\delta}_n)dt. \tag{10}$$

The system's energy loss during sinking of the contact point to reduce the contact point velocity to zero is

$$E_c = \left(\frac{m^2g^2}{2k_n}\right) + \frac{1}{2}k_n\left(\frac{mg}{k_n}\right)^2. \tag{11}$$

Here, the first term denotes the energy loss due to damping element, and the second term is the energy stored in spring element due to ground deformation, derivation of the individual terms is given in Appendix-A. Also, the post-impact energy loss due to tangential contact forces is considered negligible compared to the normal contact forces.

2.2 System's energy with ground deformation

The expression of energy derived in terms of contact point velocities is shown in Appendix-B. During leg transition, the pre-impact contact point velocities are assumed to be negligible. Hence, by neglecting the contact point velocity, we can write the energy of the pendulum in pure rotation

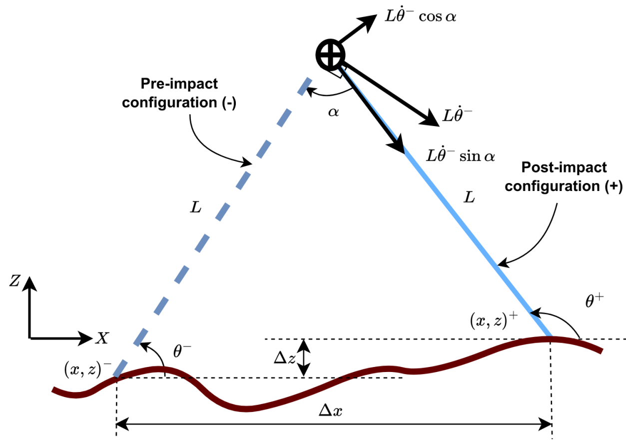

Fig. 3. Leg transition shown with both configurations i.e., pre-impact and post-impact which are denoted by (-) and (+) in the superscript

about the foot contact point as

$$E = \frac{1}{2}(I_{yy} + mL^2)\dot{\theta}^2 + mg(z + L\sin\theta). \tag{12}$$

3 LEG TRANSITION FOR WALKING

The leg transition can be considered either with continuous contact or instantaneous contact with impact. For simulating the motion, continuous contact will be considered. For foot placement planning, discrete impact event will be analyzed. The pre-impact and post-impact configurations for leg transition are shown in Fig. 3. The pre-impact terms are denoted with '-' and post-impact terms are denoted with '+' in the superscript. From Fig. 3, the relative position of contact point is given as

$$\Delta x = L\cos\theta^{-} - L\cos\theta^{+}, \tag{13}$$

$$\Delta z = L\sin\theta^{-} - L\sin\theta^{+}. \tag{14}$$

Solving for θ^- and θ^+, we get

$$\theta^+ = \text{atan2}(\Delta z, \Delta x) - \text{atan2}(\sin\alpha, \cos\alpha - 1), \tag{15}$$

$$\theta^- = \theta^+ + \alpha, \tag{16}$$

where,

$$\alpha = \text{atan2}(\pm\sqrt{4L^2(\Delta x^2 + \Delta z^2) - (\Delta x^4 + \Delta z^4) - 2\Delta x^2 \Delta z^2}, 2L^2 - (\Delta x^2 + \Delta z^2)). \tag{17}$$

Next, the two cases for support leg transition are considered to obtain the post-impact energy.

3.1 CASE-I: Energy conservation during stance foot exchange

Considering continuous contact between two configurations with energy conservation, i.e., $E^+ = E^-$, and substituting the expressions of energy as

$$mg(z + L\sin\theta^-) + \frac{1}{2}I_{yy}(\dot{\theta}^+)^2 + \frac{1}{2}m(L\dot{\theta}^-)^2 = E^-. \tag{18}$$

The angular velocity from Eq. (18) can be obtained as follows

$$\dot{\theta}^+ = \sqrt{\frac{2E^- - 2mg(z + L\sin\theta^-) - (mL^2)(\dot{\theta}^-)^2}{I_{yy}}}. \tag{19}$$

3.2 CASE-II: Energy lost in impact during stance foot exchange

The conservation of angular momentum about the contact point [22] gives

$$(I_{yy} + mL^2)\dot{\theta}^+ = (I_{yy} + mL^2\cos\alpha)\dot{\theta}^-. \tag{20}$$

The post-impact angular velocity is written as

$$\dot{\theta}^{+} = \dot{\theta}^{-} \cos\phi, \tag{21}$$

where,

$$\cos\phi = \frac{I_{yy} + mL^2 \cos\alpha}{I_{yy} + mL^2} \tag{22}$$

The energy loss during the change of stance leg includes potential energy loss due to ground deformation and loss of kinetic energy due to impact and is given by

$$E^{-} - E^{+} = \frac{m^2 g^2}{k_n} + \frac{1}{2}(I_{yy} + mL^2)(\dot{\theta}^{-})^2 \sin^2\phi, \tag{23}$$

where,

$$E^{-} = \frac{1}{2}(I_{yy} + mL^2)(\dot{\theta}^{-})^2 + mg(z + L\sin\theta^{-}). \tag{24}$$

The post-impact energy is given by

$$E^{+} = mg(z + L\sin\theta^{-}) + (E^{-} - mg(z + L\sin\theta^{-}))\cos^2\phi - \frac{m^2 g^2}{k_n}. \tag{25}$$

4 ENERGY ANALYSIS WITH DIFFERENT TERRAINS

The foot placement depends on the system's energy and can be planned based on the pre-impact energy configurations.

4.1 Curve of capture

The capture point [13] is the foot placement position on which the robot motion is completely stopped. This foot placement position depends on the system's energy. To obtain the capture point, the post-impact energy must be equivalent to the maximum potential energy, i.e., $E^+ = P_{max}$. By substituting the expression of energies, the relation between pre-impact energy and foot placement position is given as

$$E^- \cos^2\phi - \frac{m^2 g^2}{k_n} + mg(z + L\sin\theta^-)\sin^2\phi = mg(z + \Delta z + L - \frac{mg}{k_n}). \tag{26}$$

For a given value of Δx and Δz, the energy before impact can be obtained as

$$E^- = mg(z + L\sin\theta^-) + \frac{mg(\Delta z + L(1 - \sin\theta^-))}{\cos^2\phi}. \tag{27}$$

Using Eq. (27), the curve of capture is obtained over the reachable workspace of the NIP and shown in Fig. 4. For the given value of E^-, capture curve can be obtained by checking the energy condition in Eq. (27) for capture point $(\Delta x_{cp}, \Delta z)$ and fitting a polynomial such as

$$\Delta x_{cp} = f_{cp}(E^-, \Delta z). \tag{28}$$

The pre-impact energy must be greater than the maximum potential energy for walking forward, i.e., $E^- > mgL$ (for $z = 0, \Delta z = 0, \theta^- = 90°$) as in Eq. (27). An example of capture curve for NIP having system's energy $E^- = 1.2mgL$, with reference ground frame attached to the foot placement position $(0, 0)$ is shown in Fig. 5. The uneven terrain profile shown in Fig. 5 is obtained using MATLAB inbuilt function 'rand', which generates uniformly distributed random numbers.

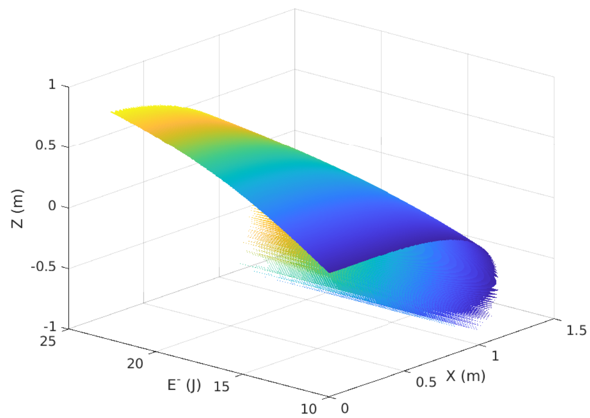

Fig. 4. Capture curve for NIP (m=1 kg, L=1 m, I_{yy}=0.33 kg m^2) on deformable terrain (k_n=7105.63 N/m, k_t=5886.93 N/m and ζ=0.6) [23]

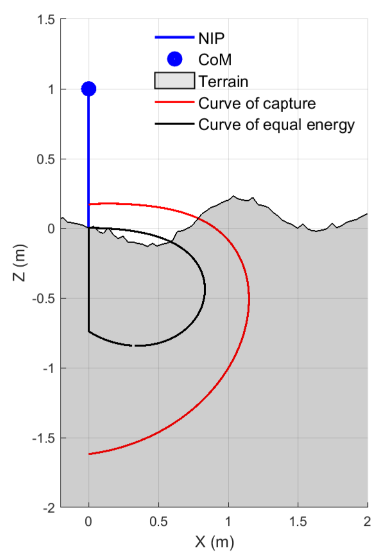

Fig. 5. Curve of capture and curve of equal local energy for system's energy $E^- = 1.2mgL$, normal stiffness k_n=7105.63 N/m, and damping ratio $\zeta = 0.6$

4.2 Curve of equal local energy

The foot placement before the capture point may increase or decrease the local energy of the system, and there is also location of foot placement at which the local energy is conserved [14]. The foot placement location at which the loss of system's energy is equal to the difference of

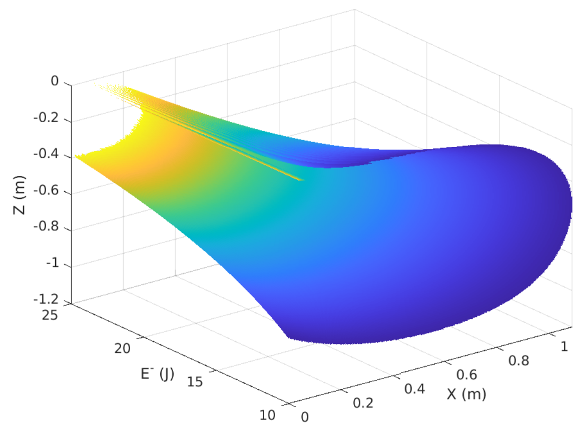

Fig. 6. Equal local energy curve for NIP (m=1 kg, L=1m, I_{yy}=0.33 kg m^2) on deformable terrain (k_n=7105.63 N/m, k_t=5886.93 N/m and ζ=0.6)

potential energy due to change of contact states is given by

$$\frac{m^2g^2}{k_n} + \frac{1}{2}(I_{yy} + mL^2)(\dot{\theta}^-)^2 \sin^2\phi = -mg(\Delta z - \frac{mg}{k_n}). \tag{29}$$

By writing the above equation in terms of pre-impact energy, we get

$$(E^- - mg(z + L\sin\theta^-))\sin^2\phi = -mg(\Delta z). \tag{30}$$

The pre-impact energy for a predefined foot placement is given by

$$E^- = mg(z + L\sin\theta^-) - \frac{mg\Delta z}{\sin^2\phi}. \tag{31}$$

Using Eq. (31), the curve of equal local energy is shown in Fig. 6.

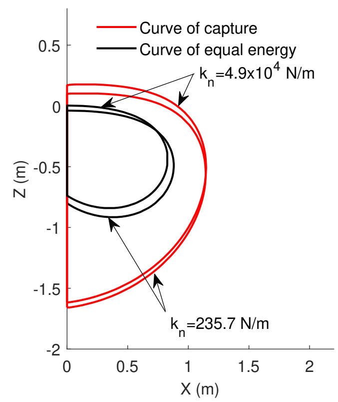

Fig. 7. Energy regions for variation of stiffness

4.3 Variation of terrain parameters

The effect of terrain properties on the energy regions is obtained by varying the stiffness and damping parameters [23] in the contact model. As the contact model parameters depend on the contact area, so the stiffness of the terrain is obtained for a flat rectangular foot of size 100 mm $\times$ 60 mm [5]. For zero rotation of the foot, the center of pressure remains at the center of the foot, which can be assumed equivalent to a point contact. The energy regions of terrain stiffness k_n=4.95×10^4 N/m and k_n=235.7 N/m for capture and equal local energy are shown in Fig. 7.

4.4 Limitation of terrain stiffness

For continuous walking on uneven deformable terrain, the kinetic energy of the system and ground deformation are related by the terrain stiffness. The curve of capture shifts downward with the increase in ground deformation, which means there exist a limitation on the terrain stiffness based on the system's energy. Let the capture point at $\Delta x = 0$ is at Δz_0, then we can write

$$\frac{F_z}{k_n} < \Delta z_0. \tag{32}$$

The terrain stiffness can be given as

$$k_n > \frac{F_z}{\Delta z_0}, \tag{33}$$

where, the normal contact force F_z from Eq. (7) is given as

$$F_z = mg + m\ddot{z} + mL\ddot{\theta}\cos\theta - mL\dot{\theta}^2\sin\theta. \tag{34}$$

Here, the minimum terrain stiffness depends on the weight, energy and dynamics of the system.

5 RESULTS

In the simulation, NIP (m=1 kg, L=1 m, I_{yy}=0.33 kg m^2) with contact forces obtained from spring-damper contact model on deformable terrain (k_n=7105.63 N/m, k_t=5886.93 N/m, and damping ratio in normal and tangential direction ζ_n=ζ_t=0.6) is considered. The motion of NIP is obtained based on the foot placement position. The step length can be adjusted in the energy regions based on the terrain height.

5.1 Foot placement on capture curve.

The intersection of the capture curve and uneven terrain is the capture point, which is the location of foot placement to stop the pendulum motion. In Fig. 8, the CoM trajectory for foot placement on the capture point is shown. The variation of kinetic and potential energy of the system is shown in Fig. 9. The kinetic energy becomes approximately zero at the maximum potential energy of the system, which is unstable equilibrium of the pendulum.

5.2 Walking with equal local energy

The foot placement on equal local energy curve maintains the same walking speed by gain of kinetic energy from loss of potential energy. The multistep simulation of NIP for foot placement

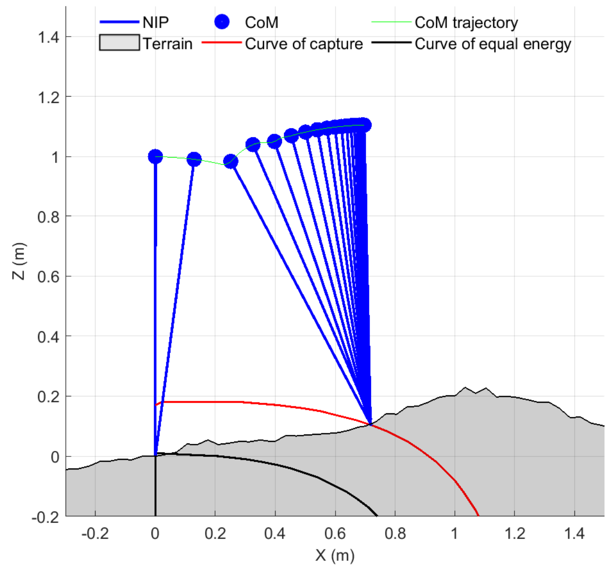

Fig. 8. Foot placement at capture point on uneven terrain based on energy regions

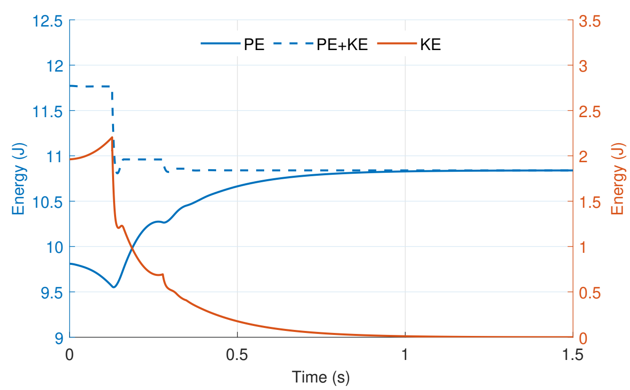

Fig. 9. Kinetic and potential energy change for foot placement at capture point on uneven terrain

at the equal local energy curve is shown in Fig. 10. Fig. 11 shows the variation of kinetic and potential energy. The energy curves are based on the impact formulation and the simulation considers the continuous contact with general motion of the NIP, hence the kinetic energy deviates from reference kinetic energy based on the numerical accuracy of simulation. This difference from the reference kinetic energy line is also denoted at points A and B in Fig. 11.

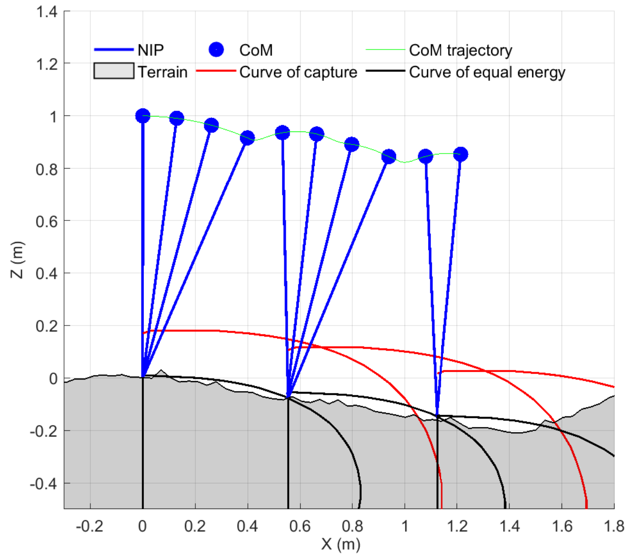

Fig. 10. Foot placement for equal local energy on uneven terrain based on energy regions

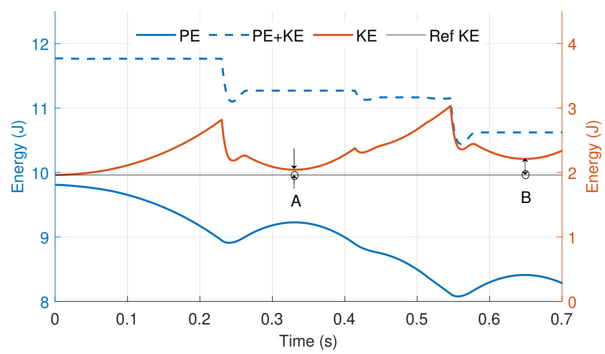

Fig. 11. Kinetic and potential energy change for foot placement at equal local energy curve on uneven terrain

5.3 Effect of variation of energy region with terrain stiffness

The foot placement on the capture point and motion of NIP on hard (k_n $=49\,564.9$ N/m) and deformable (k_n $=7105.63$ N/m) terrain are shown in Figs. 12 and 13, respectively. The capture curves are obtained without consideration of ground deformation, and the figures show the difference in the walking pattern on hard and deformable terrain. In Fig. 12, walking on hard terrain matches the energy region, whereas walking on deformable terrain by foot placement using the same energy curve has significant difference in motion as shown in Fig. 13. This implies that the energy curves obtained without considering the ground deformation will deviate the pendulum

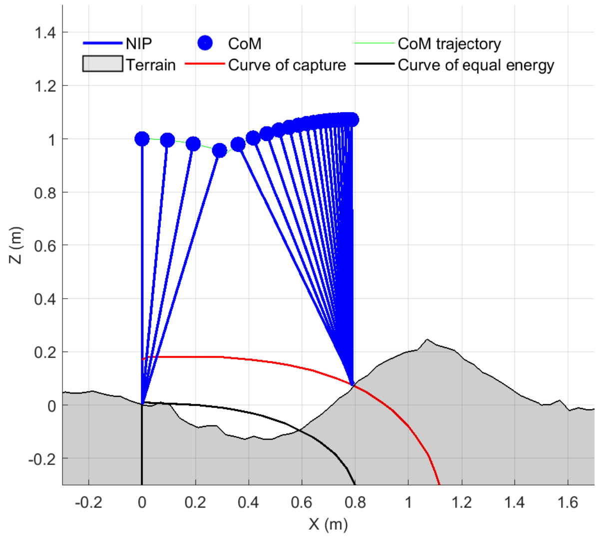

Fig. 12. Foot placement position on uneven hard terrain based on energy region obtained without ground deformation

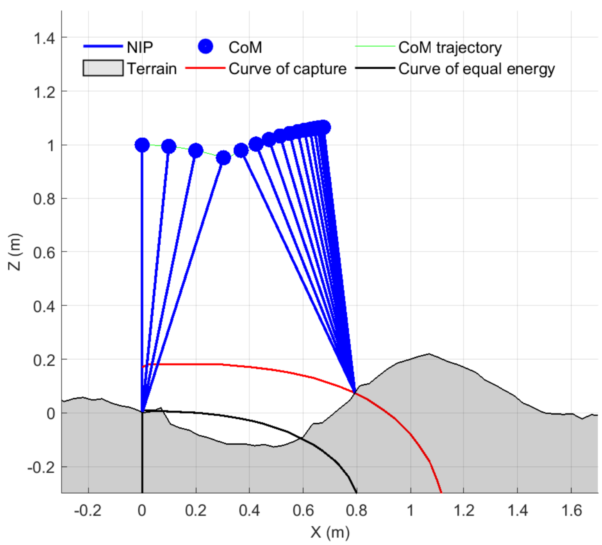

Fig. 13. Foot placement position on uneven deformable terrain based on energy region obtained without ground deformation

motion from the desired motion, and the difference will increase with decrease in terrain stiffness. The consideration of ground deformation shifts the curve based on the terrain properties. This also limits the terrain stiffness as defined in Eq. (33).

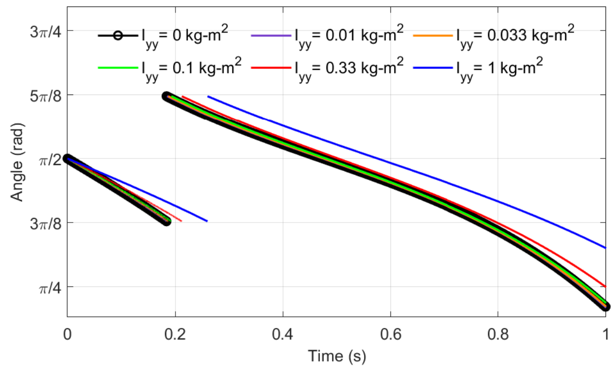

Fig. 14. Comparison of NIP models with variation in mass moment of inertia for walking on flat hard terrain (k_n=4.95×10^4 N/m)

5.4 Effect of body inertia on NIP model

The NIP model can be compared with the existing models by reducing the mass moment of inertia. For CoM model (I_{yy} =0 kg m^2, $\ddot{x}$ = $\ddot{z}$ =0 m/s^2) [14], Eq. (7) is solved for $\ddot{\theta}$, F_x and F_z. The orientation of the pendulum for step length 0.75 m on flat hard terrain with variation of mass moment of inertia is shown in Fig. 14. It is evident from Fig. 14 that as the mass moment of inertia reduces, the NIP model converges to the CoM model.

6 CONCLUSION

In this work, the center of mass model is extended for linear and rotational motion of NIP with the foot contact forces acting at the moving foot-terrain contact point. The NIP with mass moment of inertia can generate biped gait on different types of terrain without constraining the foot contact forces. Based on the system's energy and leg transition with impact, the foot placement planning on uneven deformable terrain is presented. The rigid body dynamics of NIP with spring-damper contact model is used for trajectory generation. The results show that the energy regions vary with the terrain deformation and that passive walking has limitation that depends on terrain stiffness. The limitation and variation of terrain stiffness have also been obtained. In future work, the 3D NIP motion trajectory generated for known terrain parameters will be implemented on a biped robot having 12 degrees of freedom (DOFs).

REFERENCES

[1] Vukobratović, M., and Borovac, B., 2004. "Zero-moment point—thirty five years of its life". *International journal of humanoid robotics,* **1**(01), pp. 157–173.

[2] Kajita, S., and Tani, K., 1991. "Study of dynamic biped locomotion on rugged terrain-derivation and application of the linear inverted pendulum mode". In Proceedings. 1991 IEEE International Conference on Robotics and Automation, IEEE Computer Society, pp. 1405–1406.

[3] Kajita, S., Kanehiro, F., Kaneko, K., Yokoi, K., and Hirukawa, H., 2001. "The 3d linear inverted pendulum mode: A simple modeling for a biped walking pattern generation". In Proceedings 2001 IEEE/RSJ International Conference on Intelligent Robots and Systems. Expanding the Societal Role of Robotics in the the Next Millennium (Cat. No. 01CH37180), Vol. 1, IEEE, pp. 239–246.

[4] Sato, T., Sakaino, S., Ohashi, E., and Ohnishi, K., 2010. "Walking trajectory planning on stairs using virtual slope for biped robots". *IEEE transactions on industrial electronics,* **58**(4), pp. 1385–1396.

[5] Sarkar, A., and Dutta, A., 2015. "8-dof biped robot with compliant-links". *Robotics and Autonomous Systems,* **63**, pp. 57–67.

[6] Kumar, J., and Dutta, A., 2022. "Energy optimal motion planning of a 14-dof biped robot on 3d terrain using a new speed function incorporating biped dynamics and terrain geometry". *Robotica,* **40**(2), pp. 250–278.

[7] Kajita, S., Hirukawa, H., Harada, K., and Yokoi, K., 2014. *Introduction to humanoid robotics*, Vol. 101. Springer.

[8] Lee, S.-H., and Goswami, A., 2007. "Reaction mass pendulum (rmp): An explicit model for centroidal angular momentum of humanoid robots". In Proceedings 2007 IEEE International Conference on Robotics and Automation, IEEE, pp. 4667–4672.

[9] Peng, W. Z., Song, H., and Kim, J. H., 2021. "Stability region-based analysis of walking and push recovery control". *Journal of Mechanisms and Robotics,* **13**(3).

[10] McGeer, T., 1990. "Passive dynamic walking". *Int. J. Robotics Res.,* **9**(2), pp. 62–82.

[11] Geyer, H., Seyfarth, A., and Blickhan, R., 2006. "Compliant leg behaviour explains basic dynamics of walking and running". *Proceedings of the Royal Society B: Biological Sciences,* **273**(1603), pp. 2861–2867.

[12] Goswami, A., Thuilot, B., and Espiau, B., 1996. "Compass-like biped robot part i: Stability and bifurcation of passive gaits". PhD thesis, INRIA.

[13] Pratt, J., Carff, J., Drakunov, S., and Goswami, A., 2006. "Capture point: A step toward humanoid push recovery". In 2006 6th IEEE-RAS international conference on humanoid robots, IEEE, pp. 200–207.

[14] Crews, S., and Travers, M., 2020. "Energy management through footstep selection for bipedal robots". *IEEE Robotics and Automation Letters,* **5**(4), pp. 5485–5493.

[15] Zheng, Y. F., Wang, H., Li, S., Liu, Y., Orin, D., Sohn, K., Jun, Y., and Oh, P., 2013. "Humanoid robots walking on grass, sands and rocks". In 2013 IEEE Conference on Technologies for Practical Robot Applications (TePRA), IEEE, pp. 1–6.

[16] Hashimoto, K., Kang, H.-j., Nakamura, M., Falotico, E., Lim, H.-o., Takanishi, A., Laschi, C., Dario, P., and Berthoz, A., 2012. "Realization of biped walking on soft ground with stabilization control based on gait analysis". In 2012 IEEE/RSJ International Conference on Intelligent Robots and Systems, IEEE, pp. 2064–2069.

[17] Mesesan, G., Englsberger, J., Garofalo, G., Ott, C., and Albu-Schäffer, A., 2019. "Dynamic walking on compliant and uneven terrain using dcm and passivity-based whole-body control". In 2019 IEEE-RAS 19th International Conference on Humanoid Robots (Humanoids), IEEE, pp. 25–32.

[18] Gora, S., Gupta, S. S., and Dutta, A., 2021. "Optimal gait generation of an 8-dof biped robot on deformable terrain using floating-base dynamics". In Proceedings of the Advances in Robotics - 5th International Conference of The Robotics Society.

[19] Byl, K., and Tedrake, R., 2008. "Approximate optimal control of the compass gait on rough terrain". In 2008 IEEE International Conference on Robotics and Automation, IEEE, pp. 1258–1263.

[20] Vanderborght, B., Verrelst, B., Van Ham, R., Van Damme, M., and Lefeber, D., 2008. "Ob-

jective locomotion parameters based inverted pendulum trajectory generator". *Robotics and Autonomous systems,* **56**(9), pp. 738–750.

[21] Mummolo, C., Peng, W. Z., Gonzalez, C., and Kim, J. H., 2018. "Contact-dependent balance stability of biped robots". *Journal of Mechanisms and Robotics,* **10**(2), p. 021009.

[22] Coleman, M. J., 2010. "Dynamics and stability of a rimless spoked wheel: a simple 2d system with impacts". *Dynamical Systems,* **25**(2), pp. 215–238.

[23] Lambe, T. W., and Whitman, R. V., 1991. *Soil mechanics*, Vol. 10. John Wiley & Sons.

APPENDIX A: ENERGY LOSS IN DAMPING

The deformation of the terrain increases the contact forces and reduces the contact point velocity. In case of negligible contact point velocities, the rotation of the pendulum is about the contact point. The deformation of the terrain or displacement of the contact point to support the weight of the NIP is

$$\delta_n = -\frac{mg}{k_n}. \tag{35}$$

The potential energy loss due to terrain deformation is given by

$$E_c = mg\left(\frac{mg}{k_n}\right) \Rightarrow E_c = \frac{m^2g^2}{k_n}. \tag{36}$$

The energy stored in spring element can be written as

$$E_{spring} = \frac{1}{2}k_n\left(\frac{mg}{k_n}\right)^2 \Rightarrow E_{spring} = \frac{m^2g^2}{2k_n}. \tag{37}$$

Then, the energy loss in damping is

$$E_{damping} = E_c - E_{spring} \Rightarrow E_{damping} = \frac{m^2g^2}{2k_n}. \tag{38}$$

APPENDIX B: ENERGY OF THE NONLINEAR INVERTED PENDULUM

The energy of the system (excluding the spring-damper element of contact model) is given by

$$E = \frac{1}{2}mv_{com}^2 + \frac{1}{2}I_{yy}\dot{\theta}^2 + mg(z + L\sin\theta). \tag{39}$$

The system's energy in terms of contact point parameters is obtained by substituting the velocities of center of mass from Eq. (2) in Eq. (39), as

$$E = \frac{1}{2}m((\dot{x} - L\dot{\theta}\sin\theta)^2 + (\dot{z} + L\dot{\theta}\cos\theta)^2) + \frac{1}{2}I_{yy}\dot{\theta}^2 + mg(z + L\sin\theta). \tag{40}$$

LIST OF FIGURES